Research Square

Preprints are preliminary reports that have not undergone peer review.
They should not be considered conclusive, used to inform clinical practice,
or referenced by the media as validated information.

Effect of irradiation geometry and pulse duration on laser damage thresholds of films on transparent substrates

J Camilo Diaz B

camilod@ciop.unlp.edu.ar

Centro de Investigaciones Ópticas (CONICET-CIC-UNLP)

Gabriel Bilmes

Centro de Investigaciones Ópticas (CONICET-CIC-UNLP)

Research Article

Keywords:

Posted Date: October 27th, 2026

DOI: https://doi.org/10.21203/rs.3.rs-11013121/v1

License: This work is licensed under a Creative Commons Attribution 4.0 International License.
Read Full License

Additional Declarations: No competing interests reported.

Abstract

The laser-induced damage threshold fluence (Fth) of black and aluminum paints deposited on glass substrates was investigated using femtosecond and nanosecond laser pulses under front-side (FS) and back-side (BS) irradiation geometries. Two techniques were used: Laser Ablation Induced Photoacoustics (LAIP) for FS irradiation, and Laser-Affected Area Imaging, a method introduced here, for BS irradiation. With this method we determined for the first time BS-Fth. The results show that Fth depends strongly on irradiation geometry and pulse duration. Under FS irradiation, ablation proceeds mainly by thermal vaporization. Under BS irradiation, coating damage is still observed at fluences below the ablation threshold and is attributed to photomechanical spallation. The resulting BS spallation thresholds were always lower than the FS ablation thresholds for both materials and both pulse durations. In addition, Fth was substantially lower for fs than for ns pulses. Under FS irradiation with fs pulses, Fth was the same for both paints, whereas for ns pulses the black paint threshold was approximately 30% lower than that of the aluminum paint. This indicates that the optical properties of the coating play an important role in the ns regime but are not significant in the fs regime. These results are relevant to applications involving the removal or cleaning of films deposited on transparent substrates; specifically, BS irradiation with fs pulses provides a substantially lower-fluence route for coating removal than FS irradiation.

1. Introduction

Laser ablation of thin-film coatings from transparent substrates finds applications in many fields, such as selective decoating for display manufacturing and photovoltaics [1], laser-induced forward transfer (LIFT) for printed electronics [2], pulsed laser deposition (PLD) [3], and heritage conservation, where aged coatings must be removed from historical glassware in a controlled way without mechanical or chemical contact [4], among others. These techniques must be carried out within a processing window in which the incident fluence exceeds the ablation threshold fluence of the film but remains below the laser-induced damage threshold of the transparent substrate. For common glass-paint systems, this window spans roughly one order of magnitude [5].

Within this window, the efficiency of these applications is affected by the laser pulse duration and by the choice of irradiation geometry, front side (FS) or back side (BS). In FS geometry, the laser beam impinges directly on the exposed paint surface, whereas in BS geometry the beam propagates through the glass substrate and reaches the coating-glass interface from below. BS irradiation has been shown to reduce dramatically the number of laser pulses required for complete film removal compared with conventional FS irradiation, for nanosecond pulses on black paint films [6].

The pulse duration, in turn, determines the physical regime of the laser-matter interaction. Nanosecond pulses operate in the thermally dominated regime: energy deposition is slower than thermal diffusion, and ablation proceeds through melting and vaporization, with a broad heat-affected zone [7, 8]. Femtosecond pulses operate under conditions of electron-lattice non-equilibrium and stress

confinement, which enables non-thermal ablation through phase explosion and photomechanical spallation at lower fluences [9, 10]. The ratio of ns to fs ablation thresholds is typically 2–5 for metals and composite materials [11], reflecting the energy lost to thermal diffusion in the ns regime.

A further factor that affects the efficiency of the laser ablation process is the optical properties of the absorbing film. A strongly absorbing layer, such as black paint, and a highly reflecting one, such as aluminum paint, represent two extremes for studying the influence of this parameter. Black paint absorbs nearly all the incident radiation within a submicrometric surface layer, whereas aluminum paint, once deposited, behaves as a first-surface metallic mirror that reflects or scatters most of the incident beam. Comparing these two systems under identical experimental conditions isolates the effect of the surface optical properties on the ablation threshold and mechanism.

The threshold fluence can be defined as the minimum fluence needed to detect a change in the material, such as damage or material modification, or a signature of an ablation process such as material ejection, plasma formation, or acoustic emission.

Several methods for determining the laser threshold fluence of materials have been reported in the literature. They can be broadly classified according to the physical quantity used to identify the onset of detectable changes in the material. The most direct approach consists of irradiating the sample with pulses of different fluence and examining the irradiated area by microscopy. Material removal can also be monitored directly with high-speed framing cameras, which record the ejection of material from the surface [12], or quantified with a quartz-crystal microbalance [13]. Gravimetric methods provide another direct approach, determining the fluence below which no measurable mass loss is detected when the target is weighed before and after irradiation with a precision balance [14]. The measurement of photoinduced electrical signals and of the charge of the ionized species generated during ablation has also been reported [15]. The ablation threshold can also be obtained from the dimensions of the ablated crater: the D^2 method extracts Fth from the fluence dependence of the crater diameter [16, 17].

Laser ablation is also accompanied by plasma formation and acoustic emission, which provide additional means of determining Fth. Photothermal deflection, or mirage detection, monitors the refractive-index changes around the irradiated surface associated with plasma formation, and is one of the earliest techniques used to investigate the dynamics of pulsed laser ablation [18–20]. Acoustic methods, such as Laser Ablation Induced Photoacoustics (LAIP), monitor the acoustic signal generated during the ablation process [21–23], and have also been applied to laser-cleaning processes [24–26]. In addition, simultaneous measurements of plasma emission and acoustic emission have been used to determine Fth for contaminants deposited on rolling steel plates, demonstrating the equivalence of optical and acoustic measurements for Fth determination [27, 28].

In this work we investigated the laser-induced damage threshold fluences of paint films deposited on glass substrates for two extreme cases, absorbing black paint and reflecting aluminum paint, as a function of the excitation pulse duration (nanosecond and femtosecond regimes) and of the irradiation geometry (front-side and back-side). Two techniques were used to obtain Fth: LAIP for front-side

irradiation, and Laser-Affected Area Imaging (LAAI), a method developed here to obtain the threshold fluence under back-side irradiation. The results are analyzed in terms of the mechanisms involved in the interaction of the laser pulse with the paint film, mainly ablation by thermal vaporization and photomechanical spallation.

2. Materials and Methods

2.1 Samples

Two coating systems representing optically extreme cases were investigated. The black paint samples consisted of a commercial carbon-zinc pigmented paint (density 1.05–1.15 g/cm³), which provides a highly absorbing coating. The aluminum paint samples consisted of a commercial paint (65% Al in solvent, density 0.90–1.05 g/cm³) that forms a first-surface aluminum metallic film upon drying (R > 85% at 1 μm). Both paints were applied by controlled coating onto 1 mm thick glass substrates, with layer thicknesses in the range 10–120 μm, measured with a universal thickness gauge (MU-214 B, Société Genevoise) and corroborated by optical coherence tomography (OCT) [29]. The glass substrate is transparent at both 1064 and 1028 nm, ensuring negligible energy deposition in the substrate for fluences below its own Fth [5].

2.2 Experimental set-up and procedures

Figure 1 shows the experimental setup used for the determination of Fth. Two laser systems with complementary pulse durations were used, under identical sample geometry and preparation conditions, to ensure direct comparability. For the nanosecond regime, a Q-switched Nd:YAG laser (λ = 1064 nm, τp = 7 ns FWHM) was employed. For the femtosecond regime, a Pharos laser system (Light Conversion, model PH1-06-1000-02-12-sp, λ = 1028 nm, τp = 160 fs FWHM) was used [30]. All experiments were performed in a single-shot configuration, to isolate single-pulse effects and eliminate incubation. A plano-convex lens was used to adjust the spot size on the sample. The fluence was controlled with calibrated neutral-density filters (0.1-2 J/cm² for ns pulses; 0.1-1 J/cm² for fs pulses) and measured with a pyroelectric energy meter (RjP-735/Rm-6600, Laser Probe Inc.) through a calibrated beam splitter, with an overall uncertainty of approximately 10%.

Laser Ablation Induced Photoacoustics (LAIP) was used to determine Fth under front-side irradiation. This technique is based on the detection of the acoustic signal generated during the laser ablation process. An electret condenser microphone (Panasonic WM-61A), positioned at a fixed distance from the irradiated spot, records the acoustic signal, which is amplified and digitized on an oscilloscope (300 MHz sampling rate). The peak-to-peak amplitude S of the first acoustic pulse was measured as a function of the incident fluence F. Single laser pulses of incrementally increasing fluence were applied to fresh, unirradiated areas of the sample, and independent measurement series were performed for each pulse duration, material, and geometry. Since S exhibits a region above Fth in which its dependence on fluence is linear, the threshold fluence can be obtained from the intersection of the fitted line with the horizontal axis [23, 31, 32].

For back-side irradiation, Fth was determined using the Laser-Affected Area Imaging (LAAI) method. This method consists of first acquiring photographs of the laser-affected area (LAA) after each single-shot irradiation with a calibrated binocular loupe. Each image is then analyzed with the ImageJ software, by converting it to 8-bit grayscale and applying an intensity threshold to isolate the completely cleared region, whose area is determined with the measurement function. The measured area is normalized to the maximum laser-affected area (MLAA), defined as the area corresponding to complete material removal, beyond which no further increase in size is observed as the fluence is raised, that is, the diameter remains constant. The MLAA was determined on thin films (~ 10 μm) by ablation in the FS geometry at fluences well above the ablation threshold. Finally, the normalized area obtained from each image is plotted as a function of the corresponding irradiation fluence.

3. Results

3.1 Front-Side Ablation Threshold Fluences

Front-side ablation thresholds (FS-Fth) were determined by LAIP with nanosecond and femtosecond laser pulses for both types of samples. Figure 2 shows representative LAIP curves, that is, the acoustic signal amplitude S as a function of the laser fluence F, for black paint, and Figure 3 presents the corresponding results for aluminum paint. Each data point corresponds to a single laser shot on an untreated area of the sample. Independent measurement series were performed, each one corresponding to a different coating thickness and represented by a different symbol. All the series share a common x-intercept. The solid lines correspond to least-squares linear fits of the above-threshold data, and their x-intercepts were used to determine the ablation threshold fluence Fth. As can be seen, for both materials, FS-Fth shows no significant dependence on the coating thickness over the range studied, 10-120 μm. This result is consistent with the behaviour previously reported for black paint [6].

3.2 Back-Side Thresholds

The LAIP technique was first evaluated for the determination of the laser-induced damage threshold fluence under BS irradiation (BS-Fth). The acoustic signals were found to be strongly attenuated, regardless of the microphone position, and did not adequately reflect the effects occurring in the absence of material removal, such as film delamination from the substrate or bulging, which nevertheless produce damage in the laser-irradiated area. BS-Fth was therefore determined by LAAI.

The lower parts of Figs. 4 and 5 show representative optical microscopy images of single-shot spots produced at different fluences on black paint under nanosecond and femtosecond irradiation, respectively, in both the FS and BS geometries. The upper parts show the LAA produced by each shot, normalized to the MLAA, plotted as a function of the fluence at which that particular image was

obtained. Figures 6 and 7 show the same for aluminum paint. Note that in some cases the images of the LAA reveal partial or complete removal of the paint.

The measured LAA as a function of the incident laser fluence exhibits a behavior characterized by three distinct regions: an initial region with little or no change, a linear region where the response increases rapidly, and a final region where the response gradually approaches a plateau. The intersection of the linear part of the curve with the x- axis defines the laser damage threshold fluence Fth, which, in the case of FS, matches the value obtained by LAIP, represented by the red vertical band.

It is worth noting that, although both LAIP and LAAI allow Fth to be determined from the intersection of the linear portion of the curve with the x-axis, this linear region is considerably shorter for LAAI than for LAIP. The reason is that in LAAI the laser-affected area is obtained from a 2D image, which does not account for the depth of the affected region; consequently, once the MLAA is reached, it no longer increases with the fluence. In LAIP, by contrast, the acoustic signal is generated throughout the whole volume interacting with the laser.

3.3 Discussion

Table 1 summarizes the results obtained for Fth in all configurations

Material	Geometry	Method	Fth (fs) (J/cm²)	Fth (ns) (J/cm²)	Dominant mechanism
Black paint	Front side (FS)	LAIP LAAI	0.20 ± 0.02	0.50 ± 0.03	Thermal vaporization. Ablation
	Back side (BS)	LAAI	0.10 ± 0.02	0.30 ± 0.03	Photomech. spallation
Al paint	Front side (FS)	LAIP LAAI	0.20 ± 0.02	0.68 ± 0.02	Thermal vaporization. Ablation
	Back side (BS)	LAAI	0.06 ± 0.01	0.33 ± 0.02	Photomech. spallation

Table 1. Front-side ablation thresholds (FS-Fth) and back-side spallation threshold (BS-Fth) for black paint and aluminum paint under for ns and fs pulse durations.

From the LAIP and LAAI measurements, the laser-affected area produced by front-side irradiation with both femtosecond and nanosecond pulses can be attributed mainly to ablation of the paint film. FS-Fth can therefore be identified with the ablation threshold fluence of the samples. The value FS-Fth(ns) = 0.50 ± 0.03 J/cm² obtained by LAIP for black paint agrees with previous measurements, 0.48 ± 0.05 J/cm² [6]. For aluminum paint, a value of FS-Fth(ns) = 0.68 ± 0.02 J/cm² was obtained, close to previous measurements on highly reflective metals such as stainless steel, 0.8 ± 0.2 J/cm² [31] and 0.76 J/cm²

[33]. The femtosecond thresholds are lower than the nanosecond ones. A value of FS-Fth(fs) = 0.20 ± 0.02 J/cm² was obtained for both materials, giving a ratio FS-Fth(ns)/FS-Fth(fs) = 2.5 for black paint and 3.5 for aluminum paint, in agreement with previous work reporting values of this ratio between 2 and 5 [11].

As can be seen in Table 1, the fs ablation thresholds of the two materials are the same, even though their optical properties differ markedly. This suggests that properties such as reflectivity and absorbance are not relevant in this regime, which can be interpreted within the framework described in the literature [34-36]. These works show that for irradiances ≥ ~10^{12} W/cm² the surface layer of any material, metal or dielectric, absorbing or reflecting, is transiently ionized before the end of the pulse. In this regime, the initial optical properties of the material, its reflectivity and absorption coefficient, cease to govern the energy coupling: once free carriers are generated, the laser energy is absorbed by the electron plasma through inverse bremsstrahlung, a mechanism independent of the optical state of the parent material. This is the case in our experiments, in which the fluence range of approximately 0.2-2 J/cm² corresponds to peak irradiances of I_0 ~ 1.25 × 10^{12} to 1.25 × 10^{13} W/cm² at τp = 160 fs.

This is not the case for ns pulses, for which the peak irradiance at F ~ 1 J/cm² is only ~1.4 × 10^{8} W/cm², roughly five orders of magnitude below the threshold quoted above. Surface ionization therefore never occurs during the pulse, and the optical reflectivity remains the primary factor determining the energy coupling. This explains the measurably different ns thresholds, 0.50 J/cm² for black paint against 0.68 J/cm² for aluminum paint.

Under back-side irradiation at fluences below FS-Fth, modification of the material does take place, leading to the formation of a damaged region, but no evidence of ablation was observed, such as material vaporization, plasma formation, or acoustic emission. As can be seen in Figs. 4 to 7, this behaviour persists up to BS-Fth, for both pulse duration regimes and both materials. In this fluence region, although the areas are normalized to the maximum area obtained under front-side irradiation and the plateau is reached at that MLAA, the laser-affected area produced from the back side exceeds it by more than 40%.

A more detailed microscopic analysis of the laser-affected area generated by back-side irradiation at fluences well below FS-Fth, for both pulse duration regimes and both materials, reveals morphological modifications of the surface such as delamination, blistering, bulging, and film fracture. An example is shown in Fig. 8, for a single femtosecond shot of 0.15 J/cm² impinging on aluminum paint from the back side. The front-side and back-side views show clear blistering, together with peeling of the aluminum paint from the substrate. These modifications can be attributed to photomechanical spallation, and BS-Fth can accordingly be defined as the back-side spallation threshold fluence. BS-Fth is always smaller than FS-Fth for all the configurations studied (see Table 1).

When the laser pulse propagates through the transparent glass substrate in BS geometry, it is absorbed at the paint-glass interface. In this configuration, the substrate acts simultaneously as an optical transmission window and as a rigid mechanical confinement layer. The rapid heating of the material

generates a high-pressure region that cannot expand towards the rigid substrate. This mechanical confinement produces a pressure pulse much greater than that generated during unconstrained FS irradiation, applying a strong mechanical impulse to the coating. When the pressure exceeds the adhesion strength at the coating-glass interface, the film detaches by spallation [1]. Mechanical fracture and interfacial delamination require considerably less energy than bulk vaporization and therefore occur at fluences below the ablation threshold of the material.

This confinement mechanism appears to be independent of the optical properties of the film, as it takes place in both coatings and for both pulse durations.

The influence of the pulse duration can also be understood within the framework of stress confinement theory [9, 10]. For femtosecond pulses, the laser energy is deposited before the stress wave can propagate away from the absorption region, which maximizes the peak pressure produced per unit fluence. Nanosecond pulses, in contrast, deposit the energy over a much longer time interval, allowing partial stress relaxation during irradiation and therefore producing a lower peak pressure at the same fluence. Consequently, a higher fluence is required to induce spallation with nanosecond pulses, which explains why BS-Fth is lower for fs than for ns irradiation.

4. Conclusions

The laser-induced damage threshold fluence of absorbing black and reflecting aluminum paints deposited on glass substrates was investigated using femtosecond and nanosecond laser pulses, under front-side and back-side irradiation geometries.

Two methods, Laser-Affected Area Imaging (LAAI) and LAIP, were used for characterizing the effects of laser irradiation on coating–glass systems. This combination provides a physical framework for characterizing the damage threshold in these systems. LAAI was found to be suitable for determining the threshold fluence under back-side irradiation. Its validity was assessed by applying the same analysis to front-side irradiation and comparing the resulting threshold fluences with those obtained independently using LAIP. The two methods yielded consistent threshold values for the front-side configuration, supporting the use of LAAI image analysis for determining the back-side threshold fluence. With this method we determined for the first time BS-Fth.

Results show that Fth strongly depends on irradiation geometry and pulse duration. Regarding the irradiation geometry, the processes occurring under front-side and back-side irradiation are essentially different. Under FS irradiation, ablation by thermal vaporization is the main mechanism, and therefore Fth corresponds to the ablation threshold. By contrast, under BS irradiation, coating damage is still observed at fluences below this ablation threshold. This result can be explained, as previously proposed [6], by assuming that the underlying mechanism involves the formation of a nearly isochorically superheated layer, which bends upward due to the impossibility of expanding laterally. This confinement leads to photomechanical spallation induced by the huge stress wave generated at the coating–glass interface. It is worth noting that, the laser-affected area produced under BS irradiation is more than 40%

larger than that obtained at the same fluence under FS irradiation in all cases, for both pulse-duration regimes and both materials. Besides, the resulting back-side spallation threshold fluences were at least a factor of two lower than the front-side ablation thresholds for both materials and pulse durations.

With respect to pulse duration, for both materials and geometries the Fth obtained with fs pulses is always lower than for ns pulses. This can be attributed to the way in which the film absorbs the energy of the pulse in each case. With fs pulses, the entire pulse energy is deposited locally within the irradiated area in a time much shorter than the thermal diffusion time of the material. In contrast, with ns pulses, part of the pulse energy is thermally diffused into a region larger than the irradiated area. Consequently, the fluence required to induce damage in the material is lower for fs pulses than for ns pulses. On the other hand, the ablation threshold obtained under front-side irradiation with femtosecond pulses is the same for both black and aluminum paints. In contrast, this is not the case for nanosecond pulses, for which the Fth of the black paint is approximately 30% lower than that of the aluminum paint. This means that the coating optical properties did not play an important role under fs irradiation but is relevant in the ns case.

The results obtained in this work are relevant for applications involving the removal or cleaning of films deposited on transparent substrates. In this sense, back-side irradiation with femtosecond pulses provides a substantially lower-fluence route for coating removal compared with front-side irradiation. Moreover, minimizing the irradiation fluence reduces the risk of potential substrate damage.

Declarations

Author Contribution

C.D. and G.B conceived and designed the experiments. C.D. performed the laser irradiation experiments and the LAIP and LAAI measurements. C.D. and G.B analyzed the data. C.D. prepared figures 1–8 and wrote the main manuscript text. G.B supervised the work. All authors reviewed and approved the manuscript.

Acknowledgement

The authors thank to the Laboratorio de Fotónica y Optoelectrónica (LPO) of the Instituto Balseiro & Centro Atomico Bariloche and Dinámica Estructural Ultrarrápida of the Universidad Nacional de San Martín (UNSAM) group for providing access to the facilities where the experiments involving femtosecond laser pulses were carried out. The authors also thank the Laboratorio de Optoelectrónica y Metrología Aplicada of the Facultad Regional Delta, Universidad Tecnológica Nacional (UTN), and CEMECA-CIC for their assistance with the measurements of the paint layer thickness.

References

1. G. Paltauf, P.E. Dyer, Chem. Rev. **103**, 487 (2003). https://doi.org/10.1021/cr010436c
2. M.N.R. Ashfold, F. Claeyssens, G.M. Fuge, S.J. Henley, Chem. Soc. Rev. **33**, 23 (2004). https://doi.org/10.1039/b207644f
3. N.A. Shepelin, Z.P. Tehrani, N. Ohannessian, C.W. Schneider, D. Pergolesi, T. Lippert, Chem. Soc. Rev. **52**, 2294 (2023). https://doi.org/10.1039/D2CS00938B
4. P. Serra, A. Piqué, Adv. Mater. Technol. **4**, 1800099 (2019). https://doi.org/10.1002/admt.201800099
5. P. Cech, J. Vanda, M.-G. Muresan, M. Mydlar, K. Pilna, J. Brajer, MM Sci. J. 2019, 3485 (2019). https://doi.org/10.17973/MMSJ.2019_12_2019118
6. G.M. Bilmes, J. Vallejo, C. Costa Vera, M.E. Garcia, Appl. Phys. A **124**, 347 (2018). https://doi.org/10.1007/s00339-018-1761-8
7. D. Bäuerle, *Laser Processing and Chemistry*, 4th edn. (Springer, Berlin, 2011)
8. B. Chimier, O. Utéza, N. Sanner, M. Sentis, T. Itina, P. Lassonde, F. Légaré, F. Vidal, J.C. Kieffer, Phys. Rev. B **84**, 094104 (2011). https://doi.org/10.1103/PhysRevB.84.094104
9. V.V. Zhakhovskii, N.A. Inogamov, Y.V. Petrov, S.I. Ashitkov, K. Nishihara, Appl. Surf. Sci. **255**, 9592 (2009). https://doi.org/10.1016/j.apsusc.2009.04.082
10. S.I. Anisimov, V.V. Zhakhovskii, N.A. Inogamov, K. Nishihara, A.M. Oparin, Y.V. Petrov, JETP Lett. **77**, 606 (2003). https://doi.org/10.1134/1.1600815
11. B.N. Chichkov, C. Momma, S. Nolte, F. von Alvensleben, A. Tünnermann, Appl. Phys. A **63**, 109 (1996). https://doi.org/10.1007/BF01567637
12. Y. Domankevitz, N.S. Nishioka, IEEE J. Quantum Electron. **26**, 2276 (1990). https://doi.org/10.1109/3.64364
13. S. Lazare, V. Granier, J. Appl. Phys. **63**, 2110 (1988). https://doi.org/10.1063/1.341091
14. D. Pietroy, Y. Di Maio, B. Moine, E. Baubeau, E. Audouard, Opt. Express. **20**, 29900 (2012). https://doi.org/10.1364/OE.20.029900
15. D. Vouagner, C. Beleznai, J.P. Girardeau-Montaut, C. Templier, H. Gonnord, Diam. Relat. Mater. **9**, 786 (2000)
16. S. Nolte, C. Momma, H. Jacobs, A. Tünnermann, B.N. Chichkov, B. Wellegehausen, H. Welling, J. Opt. Soc. Am. B **14**, 2716 (1997). https://doi.org/10.1364/JOSAB.14.002716
17. P.T. Mannion, J. Magee, E. Coyne, G.M. O'Connor, T.J. Glynn, Appl. Surf. Sci. **233**, 275 (2004). https://doi.org/10.1016/j.apsusc.2004.03.229
18. A. Mitra, R.K. Thareja, J. Mater. Sci. **34**, 615 (1999). https://doi.org/10.1023/A:1004567301546
19. J.A. Sell, D.M. Heffelfinger, P. Ventzek, R.M. Gilgenbach, Appl. Phys. Lett. **55**, 2435 (1989). https://doi.org/10.1063/1.102293
20. J.A. Sell, D.M. Heffelfinger, P.L.G. Ventzek, R.M. Gilgenbach, J. Appl. Phys. **69**, 1330 (1991). https://doi.org/10.1063/1.347268
21. H.K. Park, D. Kim, C.P. Grigoropoulos, A.C. Tam, J. Appl. Phys. **80**, 4072 (1996). https://doi.org/10.1063/1.363370

22. J. Krüger, H. Niino, A. Yabe, Appl. Surf. Sci. 197–198 (2002). https://doi.org/10.1016/S0169-4332(02)00418-X
23. D.J.O. Orzi, E.N. Morel, J.R. Torga, A.N. Roviglione, G.M. Bilmes, J. Phys. Conf. Ser. **214**, 012078 (2010). https://doi.org/10.1088/1742-6596/214/1/012078
24. M. Strlič, V.S. Šelih, J. Kolar, D. Kočar, B. Pihlar, R. Ostrowski, J. Marczak, M. Strzelec, M. Marinček, T. Vuorinen, L.-S. Johansson, Appl. Phys. A **81**, 943 (2005). https://doi.org/10.1007/s00339-005-3268-3
25. Y.F. Lu, Y.P. Lee, M.H. Hong, T.S. Low, Appl. Surf. Sci. **119**, 137 (1997). https://doi.org/10.1016/S0169-4332(97)00188-8
26. M.H. Hong, Y.F. Lu, W.D. Song, D.M. Liu, T.S. Low, in Microelectronic Packaging and Laser Processing, Proc. SPIE, vol. 3184 (SPIE, Bellingham, 1997). https://doi.org/10.1117/12.280568
27. D.J.O. Orzi, G.M. Bilmes, Appl. Spectrosc. **58**, 1475 (2004). https://doi.org/10.1366/0003702042641425
28. G.M. Bilmes, D.J.O. Orzi, O.E. Martínez, A. Lencina, Appl. Phys. B **82**, 643 (2006). https://doi.org/10.1007/s00340-005-2096-7
29. S. Cerrotta, J.R. Torga, E.N. Morel, J. Opt. Soc. Am. A **40**, C16 (2023). https://doi.org/10.1364/JOSAA.478870
30. S.-S. Wellershoff, J. Hohlfeld, J. Güdde, E. Matthias, Appl. Phys. A **69**, S99 (1999). https://doi.org/10.1007/s003399900305
31. D.J.O. Orzi, F.C. Alvira, G.M. Bilmes, Appl. Phys. A **110**, 735 (2013). https://doi.org/10.1007/s00339-012-7230-x
32. D.J.O. Orzi, G.M. Bilmes, Appl. Phys. A **122**, 770 (2016). https://doi.org/10.1007/s00339-016-0294-2
33. M. Mesaros, O.E. Martínez, G.M. Bilmes, J.O. Tocho, J. Appl. Phys. **81**, 1014 (1997). https://doi.org/10.1063/1.364196
34. E.G. Gamaly, A.V. Rode, B. Luther-Davies, V.T. Tikhonchuk, Phys. Plasmas. **9**, 949 (2002). https://doi.org/10.1063/1.1447555
35. A. Roberts, D. Cormode, C. Reynolds, T. Newhouse-Illige, B.J. LeRoy, A.S. Sandhu, Appl. Phys. Lett. **99**, 051912 (2011). https://doi.org/10.1063/1.3623760
36. T. Genieys, M. Sentis, O. Utéza, Appl. Phys. A **126**, 263 (2020). https://doi.org/10.1007/s00339-020-3440-9

Figures

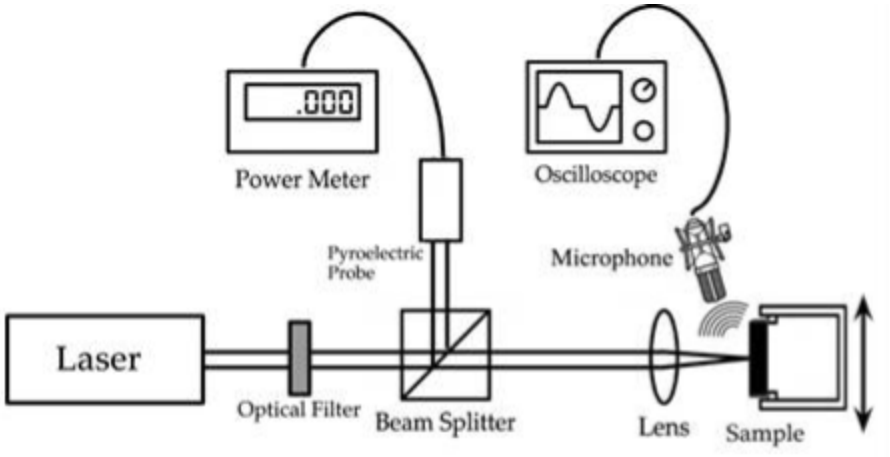


Figure 1

Experimental setup

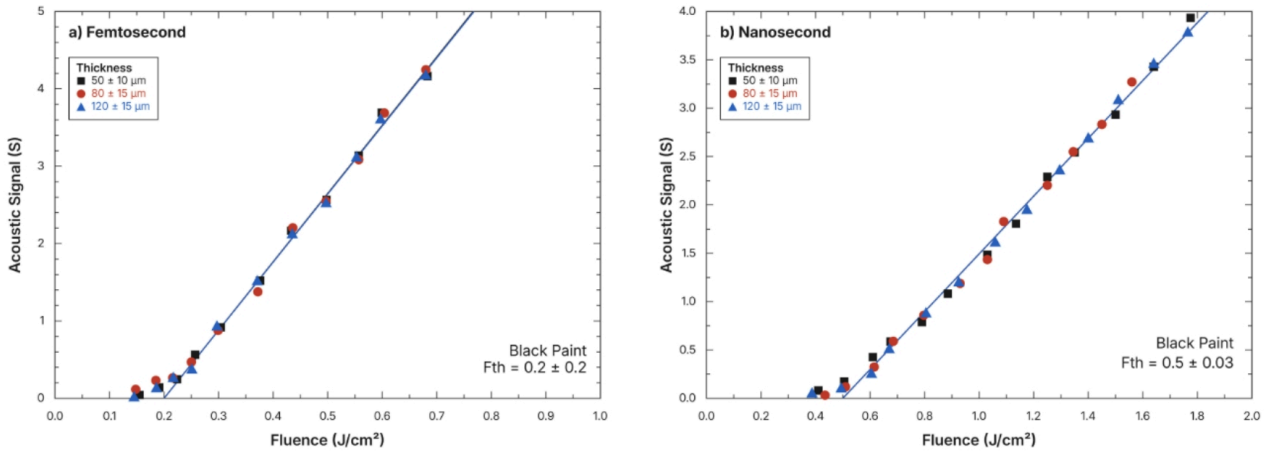


Figure 2

LAIP signal amplitude S as a function of incident fluence F for black paint under FS geometry. Left: femtosecond pulses (FS-Fth = 0.20 +/- 0.02 J/cm^2); right: nanosecond pulses (FS-Fth = 0.50 +/- 0.03 J/cm^2). Each symbol set represents an independent measurement series and corresponds to a different thickness; solid lines indicate linear fits.

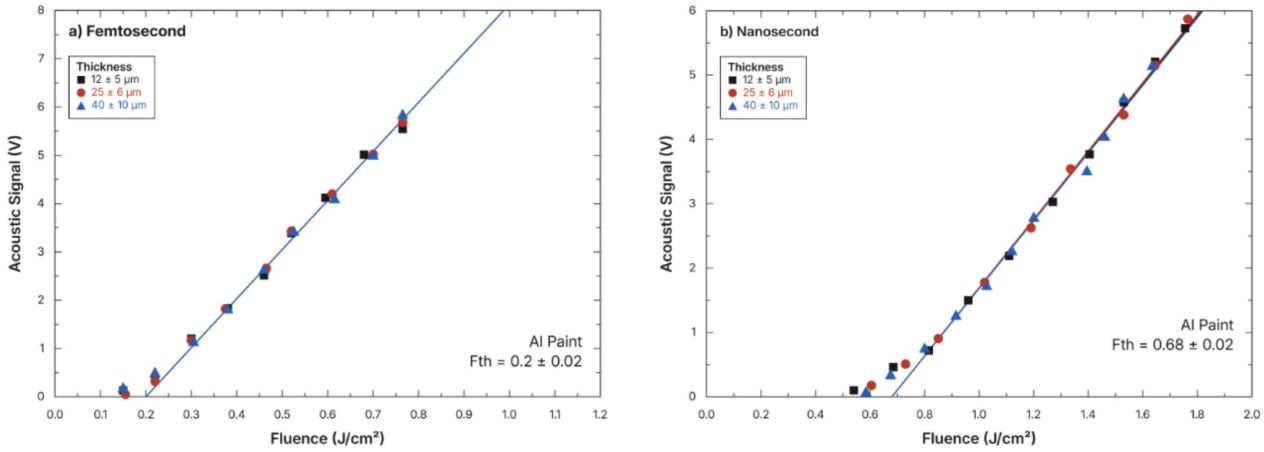


Figure 3

LAIP signal amplitude S as a function of incident fluence F for aluminum paint under FS geometry. Left: femtosecond pulses

(FS-Fth = 0.20 +/- 0.02 J/cm^2); right: nanosecond pulses (FS-Fth = 0.7 +/- 0.02 J/cm^2). Each symbol set represents an independent measurement series and corresponds to a different thickness; solid lines indicate linear fits.

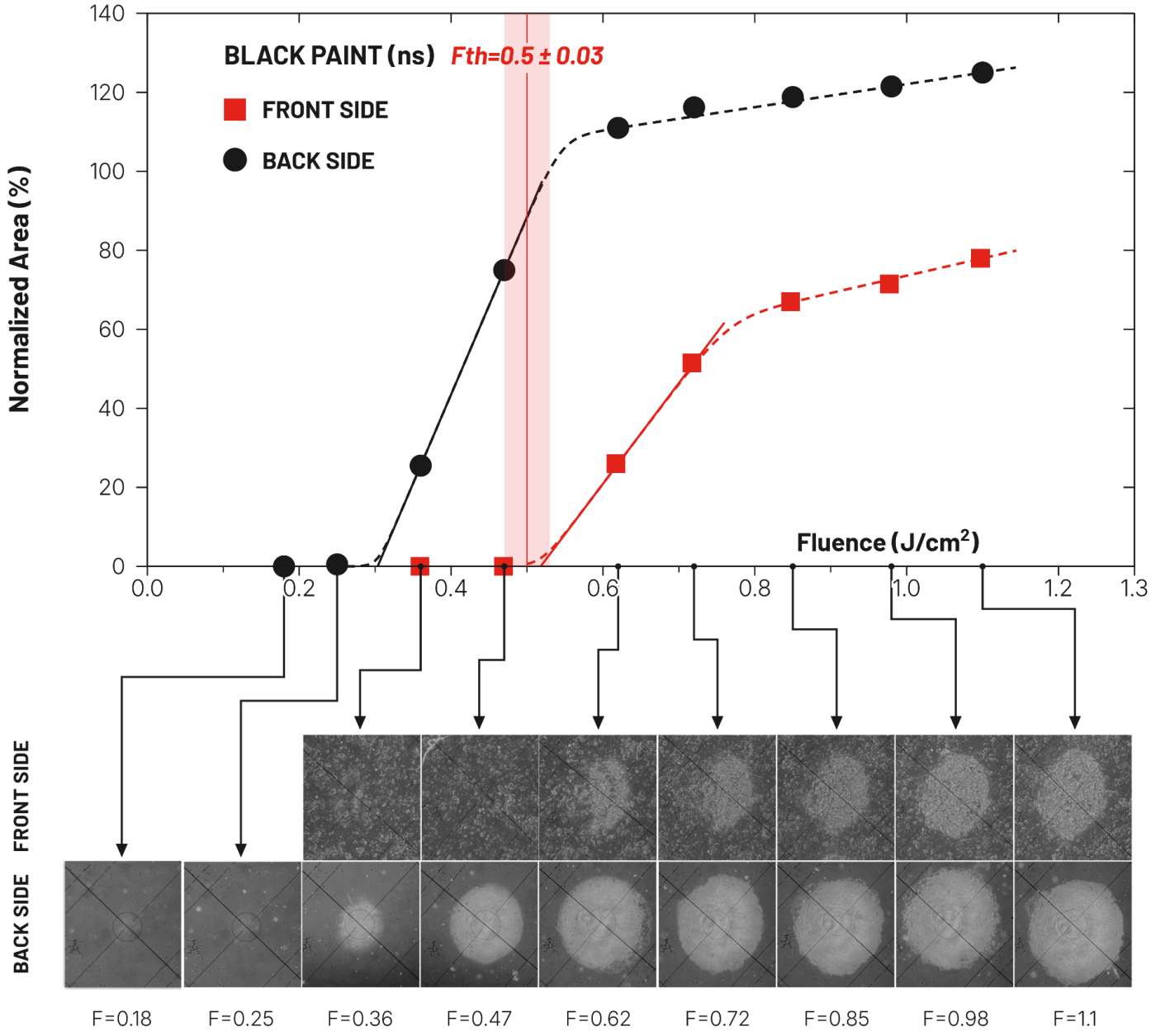


Figure 4

Lower part: optical microscopy images of single-shot interaction spots on black paint (thickness 50 ± 10 µm) under nanosecond pulses, as a function of the fluence, for the FS and BS geometries. Upper part: laser-affected area produced by each shot, normalized to the MLAA, plotted as a function of the fluence at which the corresponding image was obtained. For reference, the circle at the centre of the images corresponds to the microscope scale bar.

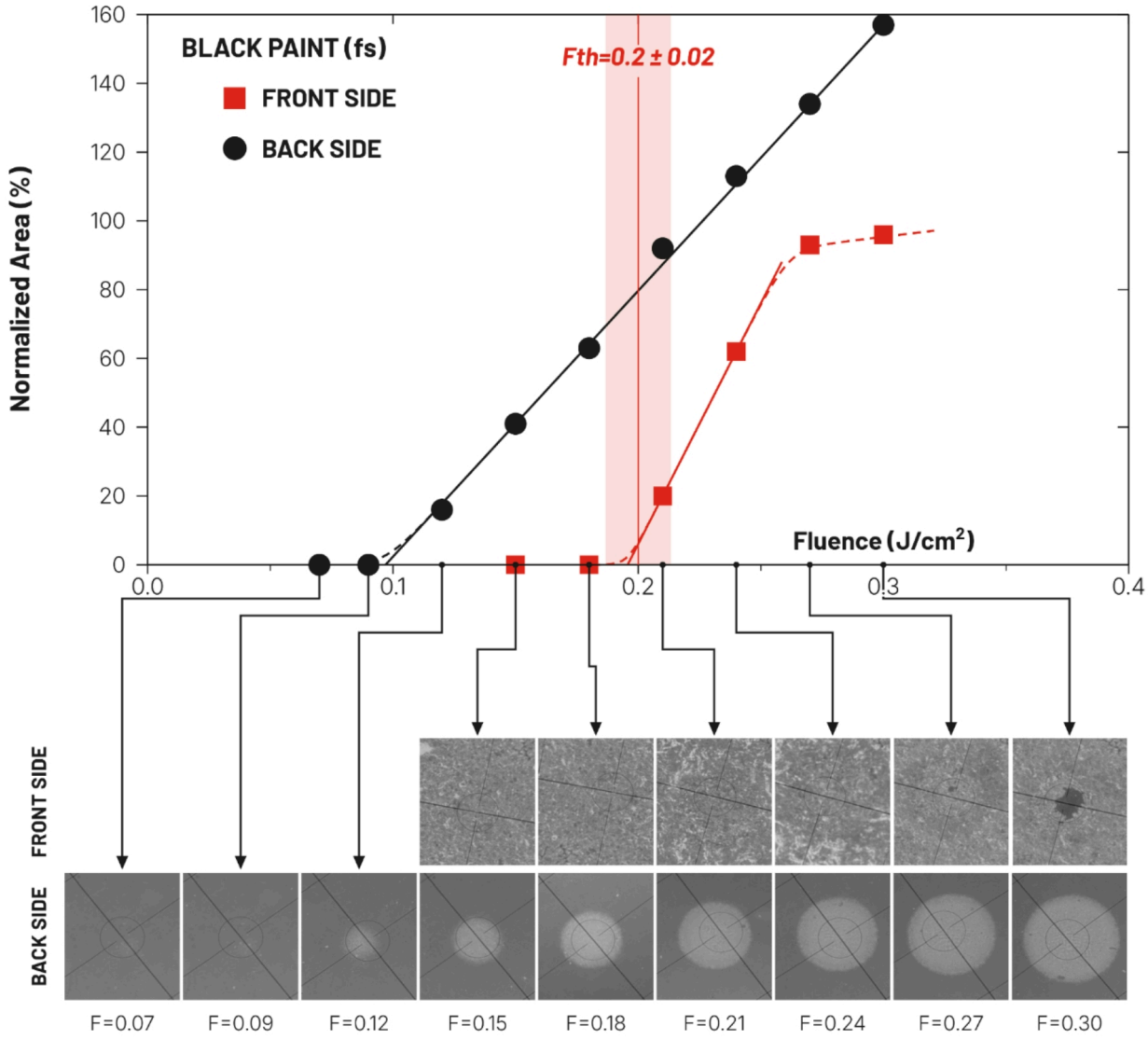


Figure 5

Lower part: optical microscopy images of single-shot interaction spots on black paint (thickness 50 ± 10 µm) under femtosecond pulses, as a function of the fluence, for the FS and BS geometries. Upper part: laser-affected area produced by each shot, normalized to the MLAA, plotted as a function of the fluence at which the corresponding image was obtained. For reference, the circle at the centre of the images corresponds to the microscope scale bar.

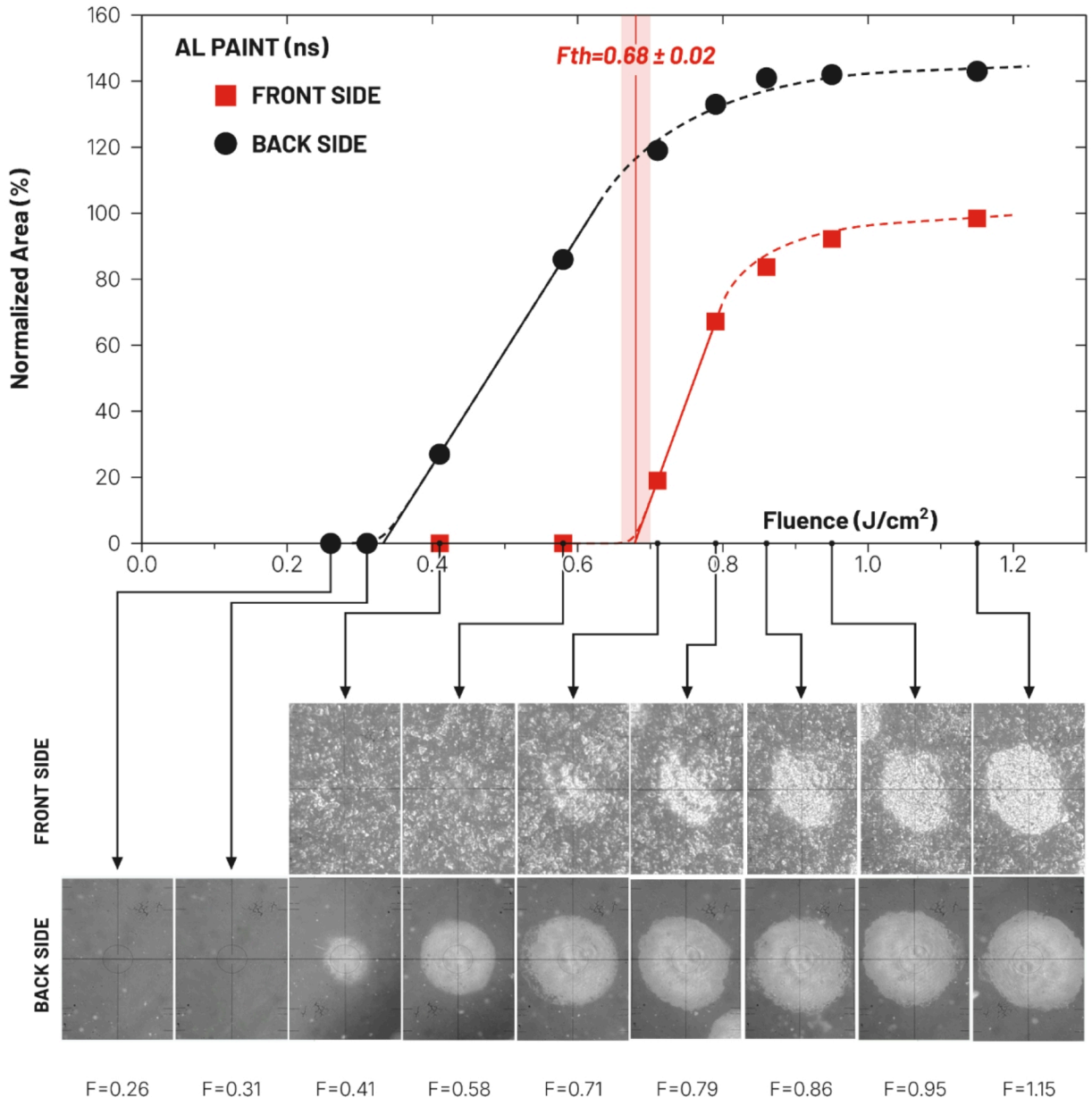


Figure 6

Lower part: optical microscopy images of single-shot interaction spots on aluminum paint (thickness 25 ± 6 μm) under nanosecond pulses, as a function of the fluence, for the FS and BS geometries. Upper part: laser-affected area produced by each shot, normalized to the MLAA, plotted as a function of the fluence at which the corresponding image was obtained. For reference, the circle at the centre of the images corresponds to the microscope scale bar.

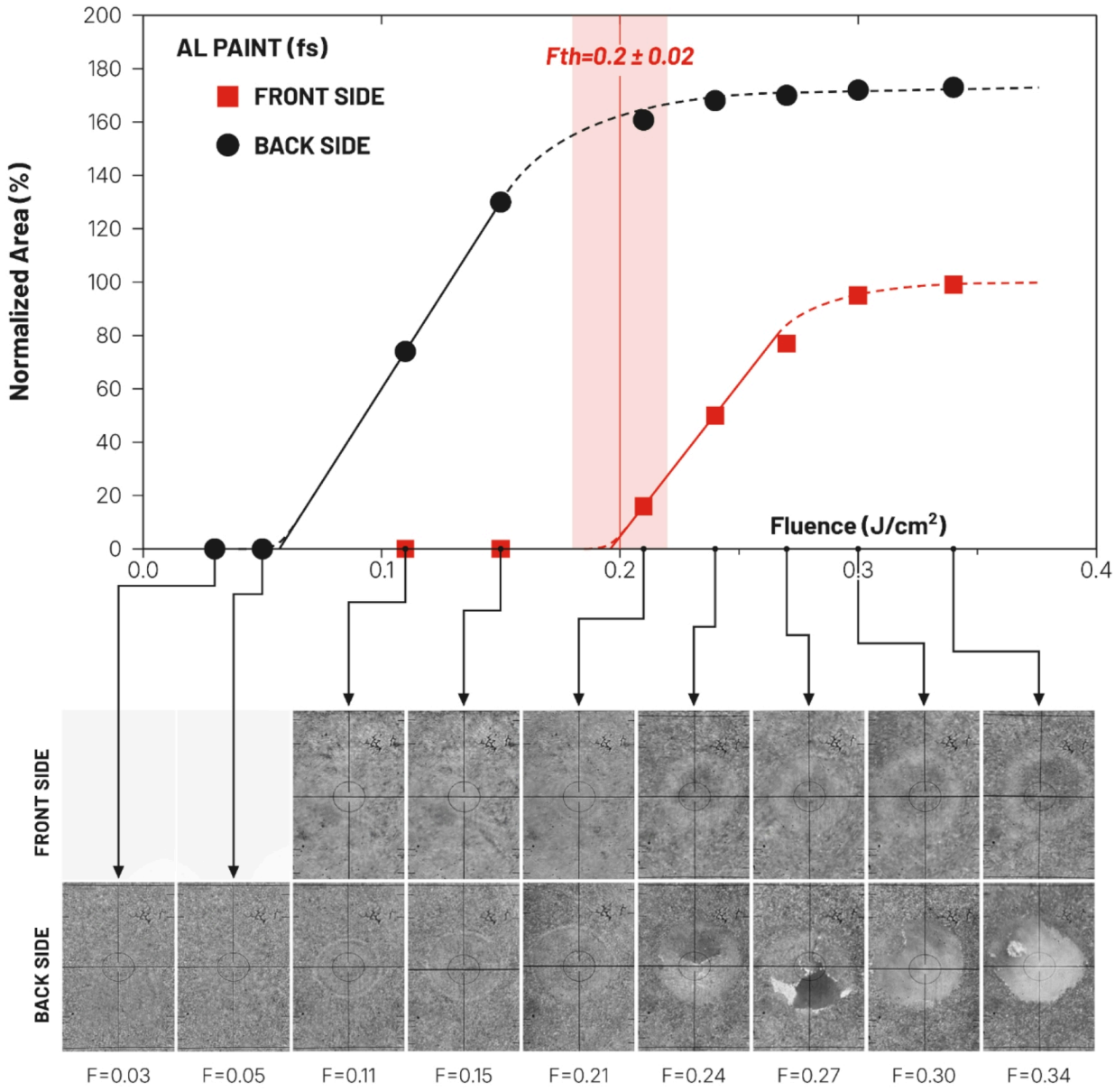


Figure 7

Lower part: optical microscopy images of single-shot interaction spots on aluminum paint (thickness 25 ± 6 μm) under femtosecond pulses, as a function of the fluence, for the FS and BS geometries. Upper part: laser-affected area produced by each shot, normalized to the MLAA, plotted as a function of the fluence at which the corresponding image was obtained. For reference, the circle at the centre of the images corresponds to the microscope scale bar.

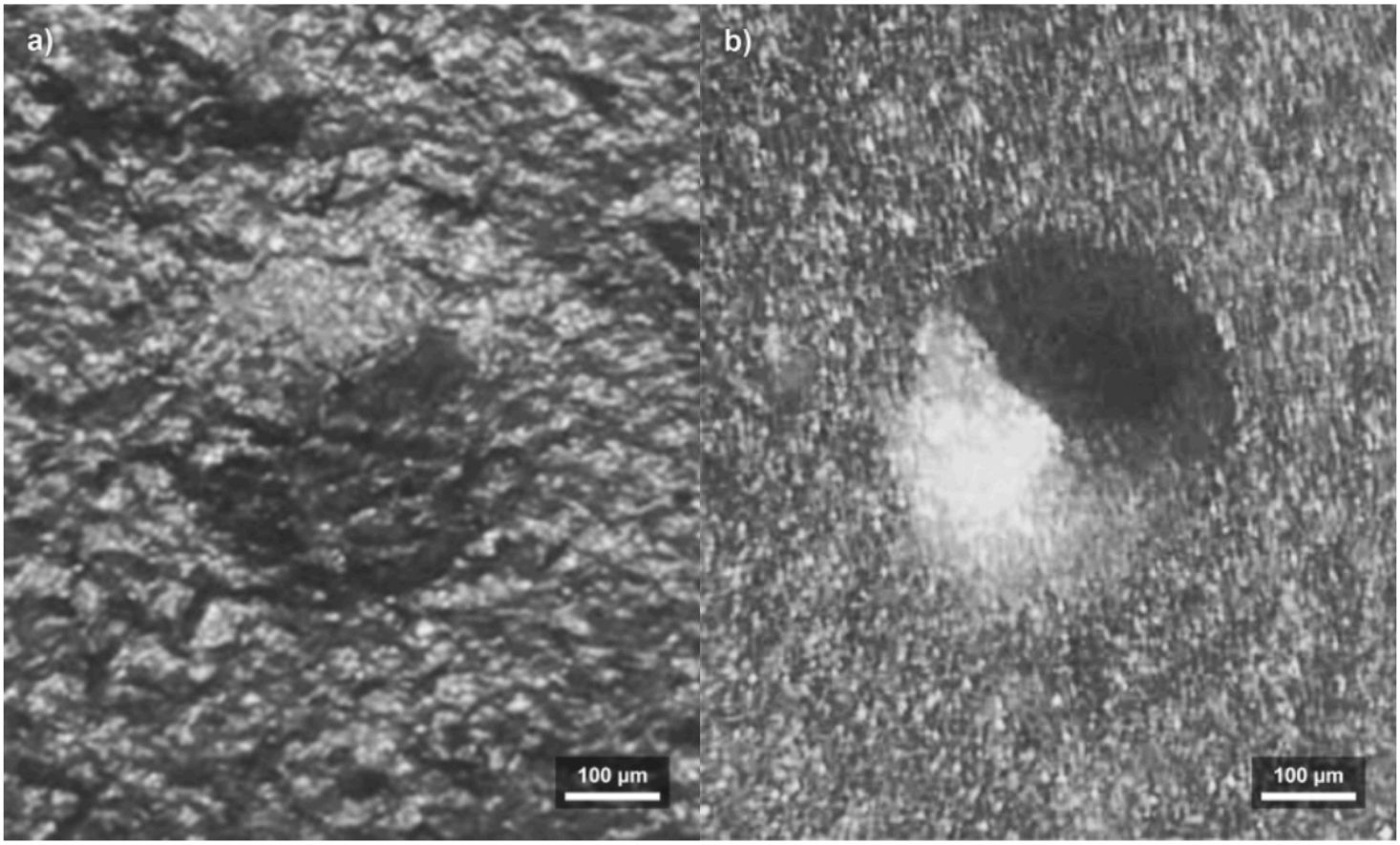


Figure 8

Images of a femtosecond single-shot of 0.15 J/cm² impinging on Al paint (thickness 40 ± 10 µm) in BS geometry a) front side view , and b) back side view